

ARTICLE OPEN



Exogenous moisture deficit fuels drought risks across China

Gang Wang^{1,2,3,11}, Qiang Zhang^{1,11}✉, Yadu Pokhrel⁴, Daniel Farinotti^{5,6}, Jida Wang⁷, Vijay P. Singh^{8,9} and Chong-Yu Xu¹⁰

Intensifying droughts under climatic warming are of widespread concern owing to their devastating impacts on water resources, societies and ecosystems. However, the effects of exogeneous drivers on regional droughts remain poorly understood. Using the Lagrangian method, atmospheric reanalysis data and climate projections from the Coupled Model Inter-comparison Project phase 6 (CMIP6), we show how exogenous precipitation minus evaporation (PME) deficit drives droughts across China. More specifically, we demonstrate that four distinct trajectories of such exogenous PME deficit fuel regional droughts. Three of these trajectories relate to oceanic PME deficit originating from the North Atlantic, eastern Bering Sea and Indian Ocean, and one trajectory characterizes exogenous terrestrial PME deficit from the Siberian Plateau. We show that during 1980–2020, droughts induced by exogenous PME deficit account for 45% of all droughts that occurred in China's coastal region, and for 7% of all droughts in the northwestern regions. Under climate scenario SSP245 (SSP585), limiting warming to 1.5 °C compared to 2 °C above pre-industrial levels could avoid 60% (84%) of exogenous drought exposure. This would in turn reduce population exposure by 40% (49%), and economic exposure by 73% (66%). Our study unravels how exogenous PME deficit drives droughts in China, underscoring the role that external drivers have on regional droughts and associated future prediction.

npj Climate and Atmospheric Science (2023)6:217; <https://doi.org/10.1038/s41612-023-00543-8>

INTRODUCTION

Droughts have become one of the world's deadliest and costliest hazards, imposing far-reaching impacts on global agricultural production and sustainable development^{1–3}. Recent decades have witnessed intensifying droughts globally⁴ including China^{5,6}, the southwestern United States^{7,8}, and Europe⁹. Over the past 50 years, droughts have caused ~650,000 deaths with global economic losses of about US\$124 billion³. Within the Sustainable Development Goals (SDGs) proposed in 2015 by the United Nations (UN), droughts are directly linked to 9 SDGs, as they threaten food security, trigger water degradation, cause ecological crisis, and lead to poverty¹⁰.

While droughts have been a topic of intensive research, most existing studies have focused on internal hydrometeorological aspects^{6,11–13}, with little attention to the external drivers. In a recent study, we correlated decreased terrestrial water storage in the mid-latitude Eurasia to precipitation minus evaporation (PME) deficit in the low-latitude North Atlantic Ocean¹⁴. Building on those findings, we now show that exogenous PME deficit could fuel regional drought risks^{15,16}.

Drought can propagate across thousands of kilometers over land and ocean^{15–17}. We use monthly PME to track droughts over medium to long time scales. However, the fractional contribution of exogenous PME deficit-induced droughts (hereafter referred to as “exogenous droughts”) to overall droughts remains poorly quantified^{15,18}. Here we distinguish exogenous droughts from endogenous droughts (i.e., droughts originating internally to a given region) and evaluate the impacts of the two type of droughts from historical and future viewpoints.

Drought propagation is closely related to anomalous water vapor transport via large-scale atmospheric circulation^{14,19}, coupled land-atmosphere feedback^{18,20,21}, and surface temperature field²². We backtrack the propagation trajectories of PME deficit, unraveling the sources of PME deficit-droughts and their impacts on regional drought conditions². Specifically, we use the Lagrange technique to backtrack trajectories and categorize the propagation pathways of exogenous PME deficit using a random forest model. We develop mechanistic links between sea surface temperature (SST)^{17,22–24} and propagation trajectories of terrestrial and oceanic PME deficit. We further use different Shared Socio-economic Pathways (SSPs) to examine future evolutions of exogenous and endogenous droughts across China and to quantify population and economic exposure to droughts. We perform these analyses for different global warming levels (GWLs), with a specific focus on scenarios implying 1.5 °C and 2 °C of warming above pre-industrial levels²⁵.

Being located in the East Eurasian monsoon zone, China is afflicted by frequent droughts^{5,6}, with profound implications on its vast agricultural systems and other economic activities^{26,27}. For example, the severe drought in Yunnan in 2010 triggered drinking water shortage for 8.1 million people and the loss of an estimated \$2.5 billion worth of grain production^{26,28}, while the drought in northern China in 2015 afflicted 21 million people and caused direct economic losses of \$1.84 billion²⁹. Mitigation of and preparedness for droughts are mostly done at the regional scale, rarely accounting for the impacts of exogenous droughts^{6,11–13}. Here, we unravel the impacts of exogeneous drivers on droughts across China, providing understanding and shedding light on regional drought risk evaluation under warming climate.

¹Advanced Interdisciplinary Institute of Environment and Ecology, Beijing Normal University, Zhuhai 519087, China. ²State Key Laboratory of Earth Surface Processes and Resource Ecology, Beijing Normal University, Beijing 100875, China. ³Faculty of Geographical Science, Beijing Normal University, Beijing 100875, China. ⁴Department of Civil and Environmental Engineering, Michigan State University, East Lansing, MI, USA. ⁵Laboratory of Hydraulics, Hydrology and Glaciology (VAW), ETH Zurich, Zurich, Switzerland. ⁶Swiss Federal Institute for Forest, Snow and Landscape Research (WSL), Birmensdorf, Switzerland. ⁷Department of Geography and Geospatial Sciences, Kansas State University, Manhattan, KS, USA. ⁸Department of Biological and Agricultural Engineering and Zachry Department of Civil & Environmental Engineering, Texas A&M University, College Station, TX 77843, USA. ⁹National Water and Energy Center, UAE University, Al Ain, United Arab Emirates. ¹⁰Department of Geosciences and Hydrology, University of Oslo, Oslo, Norway. ¹¹These authors contributed equally: Gang Wang, Qiang Zhang. ✉email: zhangq68@bnu.edu.cn

RESULTS

Exogenous droughts in China over the past 40 years

Distinguishing exogenous droughts from internally-originated droughts is a prerequisite for better understanding the drivers of regional drought conditions. Here we identify 57 exogenous droughts and 488 endogenous droughts that occurred during 1980–2020 (Fig. 1 and Supplementary Figs. 1, 2). We distinguish four propagation routes toward China from 57 trajectories of exogenous droughts by using a K-means clustering technique (see Methods). The west route starts from the mid-low latitude Atlantic and propagates eastward towards Europe, then Kazakhstan finally reaching northwestern China. The PME deficit propagating along this route amplifies droughts over the Xinjiang Province, China. The north route extends southward from Central Russia, over Mongolia, to northwestern China. Its PME deficit impacts Inner Mongolia and the Heilongjiang Province. The east route propagates westwards from the North Pacific, across the East China Sea, to coastal regions of Eastern China. The PME deficit propagating along this route exacerbates droughts over the East Coast of China. The south route, finally, originates from the South China Sea and propagates northwards across the Northern Indian Ocean, the Qinghai-Tibet Plateau (QTP), and eventually to southeastern China. The PME deficit propagating along the south route affects droughts over southeastern and southern China, whereas the Eurasian drylands are dominated by the west and north PME deficit propagation routes³⁰.

The four PME deficit propagation routes explain 21 terrestrial exogenous droughts and 32 oceanic exogenous droughts, accounting for 37% and 56% of China's total exogenous droughts from 1980 to 2020, respectively. The coastal regions of eastern China are most populous with highly-developed economies, constituting 57% of China's gross domestic product in 2018^{31,32}. However, oceanic exogenous droughts heavily affect these coastal regions, with 45% of the total droughts being of exogenous origin (Supplementary Fig. 1). Meanwhile, we identify a corridor, about 1500 km in length and stretching along the mainstem of the Yangtze River (Supplementary Figs. 2–4), which is dominated by exogenous droughts. We ascribe this dominance to the oceanic PME deficit from the Pacific Ocean, i.e., a deficit propagating along the east route (see above).

While the drought frequency is higher in central China, the total drought exposure (i.e., the duration of the droughts) is greater in southeastern China and QTP (Supplementary Fig. 5). Exogenous drought occurs most frequently in southeastern and southern China, resulting in a higher drought exposure (Fig. 1) and a strong correlation between exogenous drought exposure and frequency¹⁵. Moreover, exogenous droughts tend to last longer, and to clusters over extensive areas (Fig. 1, Supplementary Fig. 3). This is in contrast to endogenous droughts, which mainly afflict the QTP and northwestern China (Supplementary Fig. 4).

Water vapor anomalies and propagation trajectories of exogenous droughts

External, intense water vapor deficit prompted a record-breaking summer drought in southwest China in 2011, causing significant loss to the society and economy³³. Analyzing water vapor anomalies and relevant propagation trajectories, we find traces of exogenous influence for this event. In particular, we identify an exogenous driver for the drought occurring between April 2011 and June 2011, (Fig. 2, Supplementary Figs. 6–9). We observe high pressure in eastern China, and at the same time, dry updraft induced by warming SST in the northern Pacific Ocean are transported, until subsidence near China with cooling SST^{34,35}. This process resulted in abnormally low high-altitude potential height, which triggered the westward spreading of dry airmasses during the initial period of the 2011 droughts (Supplementary Figs. 6–9). In April 2011, the moisture deficit (P-E below the 20%

threshold) over the ocean triggered the drought. Anomalously high pressure later drove a westward movement of the airmasses of the lower atmosphere (Supplementary Fig. 9). In May, air masses over the upper atmosphere carry dry air and move landwards. Given the landfalling of dry airmasses, these dry airmasses can subside due to the boosting of anomalously high pressure. We view that the decrease in water vapor transport and ocean-atmosphere coupling is the main physical mechanism behind the 2011 drought genesis and propagation (Fig. 2).

To unravel the relations between PME deficit, large-scale climate variability, and SST^{14,36}, we quantify the effects of SST anomalies in the area 20°S–45°N on PME (between 60°E–145°E, 0°–60°N) during the period 1980 to 2020. We do this by using the Maximum Covariance Analysis (MCA) method (Fig. 3). The first leading MCA mode (MCA1), which we relate to SST, explains 47% of the variance in the PME variability. Indeed, the normalized PME in the first mode agrees with the SST anomaly in time (correlation = 0.73 for time lags of 2–3 months) (Fig. 3c). Moreover, the spatial pattern of the Pacific SST matches well with that of the El Niño Southern Oscillation (ENSO), and the Niño SST index 3.4 correlates strongly (correlation = 0.90) with the temporal coefficient of the first leading mode. We interpret this as an indication for the remarkable impacts that Pacific SST can have on precipitation variations over China³⁷. Also, the time series of the Pacific Decadal Oscillation (PDO) agrees with SST anomalies (correlation = 0.9). Following earlier works, we interpret this as an indication for the fact that the interannual relationship between ENSO and the regional climate can be mediated by the PDO phase³⁶. The propagation of dry airmasses during negative PDO phases, which are characterized by warm North Pacific SSTs, is consistent with the SST patterns of the exogenous drought landfalls in 2011.

Projected exogenous droughts under additional 1.5 °C and 2 °C of warming

Based on multi-model ensembled CMIP6 data, we track 647 and 662 trajectories projected for exogenous drought at GWL 1.5 °C and 2.0 °C above pre-industrial levels, respectively (Fig. 4 and Supplementary Fig. 10). The 647 projected trajectories of exogenous drought at GWL 1.5 °C under SSP585 scenario can be grouped into 4 clusters (Fig. 4). In Cluster 1 (202 trajectories, i.e., 31% of the total), exogenous droughts originate from the Pacific Ocean and land in China, impacting coastal regions of eastern China and decreasing terrestrial water storage in southern China^{38,39}. In Cluster 2 (170 trajectories, 26%), exogenous droughts mainly originate from the drylands of northern Asia, propagate into China via Mongolia, and thus afflict Inner Mongolia and parts of China. In Cluster 3 (128 trajectories, 19%), exogenous droughts propagate along a route spanning from the Atlantic, over the Mediterranean, to the Caspian Sea. This mainly happens within a mid-low latitude belt (10°N–50°N) and primarily affects western China. In Cluster 4 (162 trajectories, 24%), finally, trajectories are concentrated over Southeast Asia and the corresponding coastal regions, mostly afflicting Southwest China. In general, the trajectories of exogenous drought at GWL 2.0 °C are similar to those at GWL 1.5 °C, although there is a visible tendency for the trajectories to affect larger areas (Supplementary Fig. 11).

Future exogenous droughts tend to have more influence on southern China than on western China (Figs. 1, 4). Compared to present-day climatic conditions (1975–2014), China is expected to suffer from increased drought exposure, mostly resulting from a lengthened drought duration and an increase in the area impacted by the droughts (Supplementary Figs. 12, 13). We also note an increase in the exposure resulting from exogenous droughts when compared to endogenous droughts (Fig. 4, Supplementary Figs. 14–17). Specifically, for GWL 1.5 °C, the exogenous drought exposure across China is expected to increase by around 8% (95% confidence interval when considering both

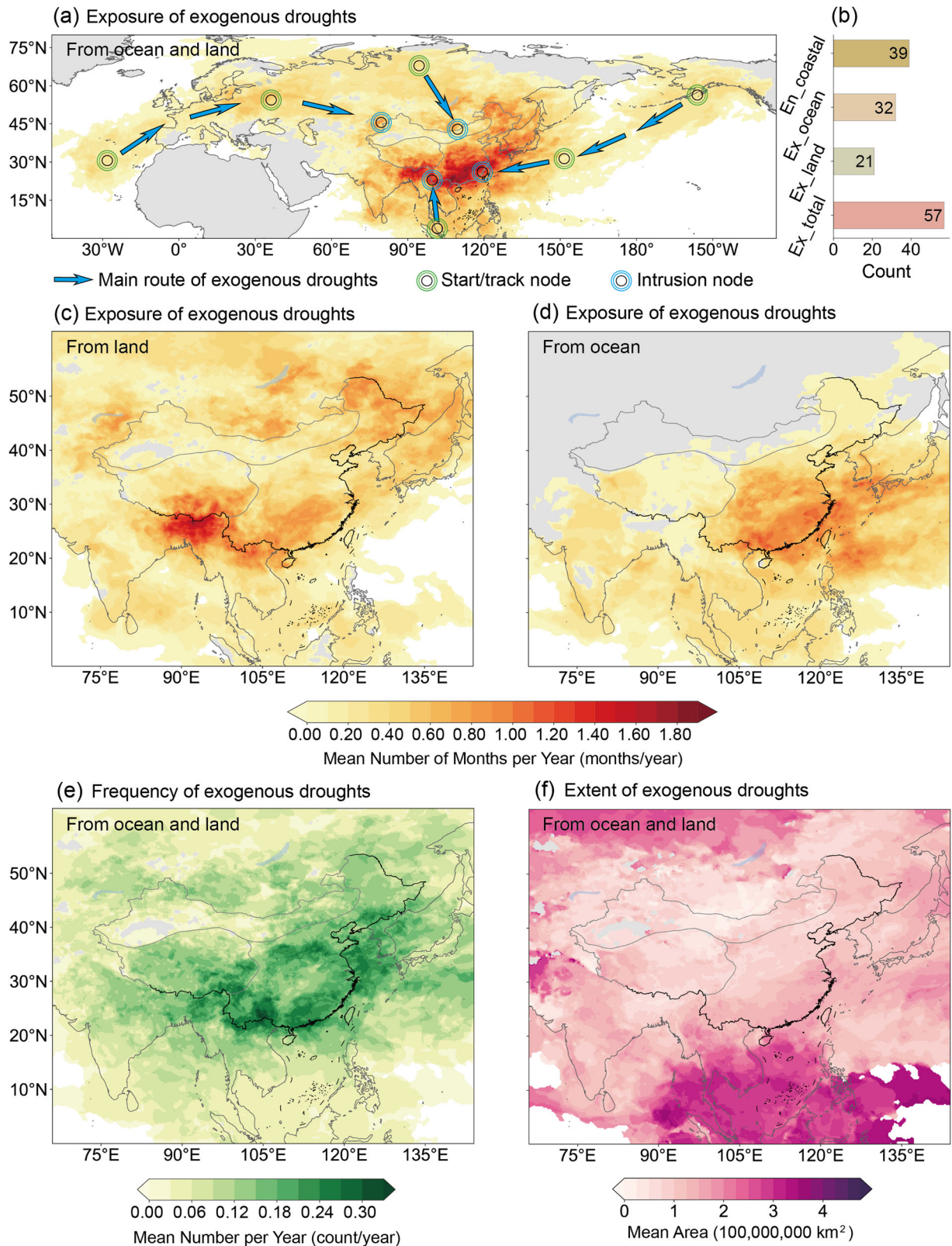


Fig. 1 Exogenous droughts in China during 1980–2020. Spatial distribution of exogenous droughts exposure from ocean and land (a), from land (c), and from ocean (d). Spatial distribution of exogenous droughts frequency (e) and extent (f) from ocean and land. Panel b provides a count of different types of droughts. Abbreviations are as follows: Ex_ocean = exogenous droughts from the ocean. En_coastal = endogenous droughts in coastal China. Ex_land = exogenous droughts from land. Ex_total: total exogenous droughts.

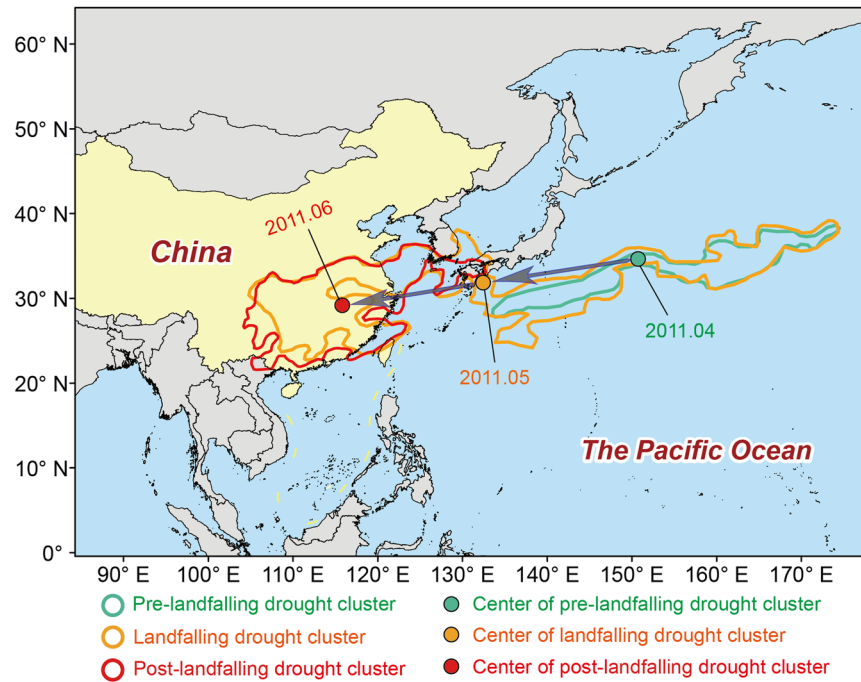


Fig. 2 The evolution processes during the onset of the exogenous 2011 drought in China (April to June 2011). Green for pre-landfalling drought cluster, yellow for landfalling drought cluster, red for post-landfalling drought cluster.

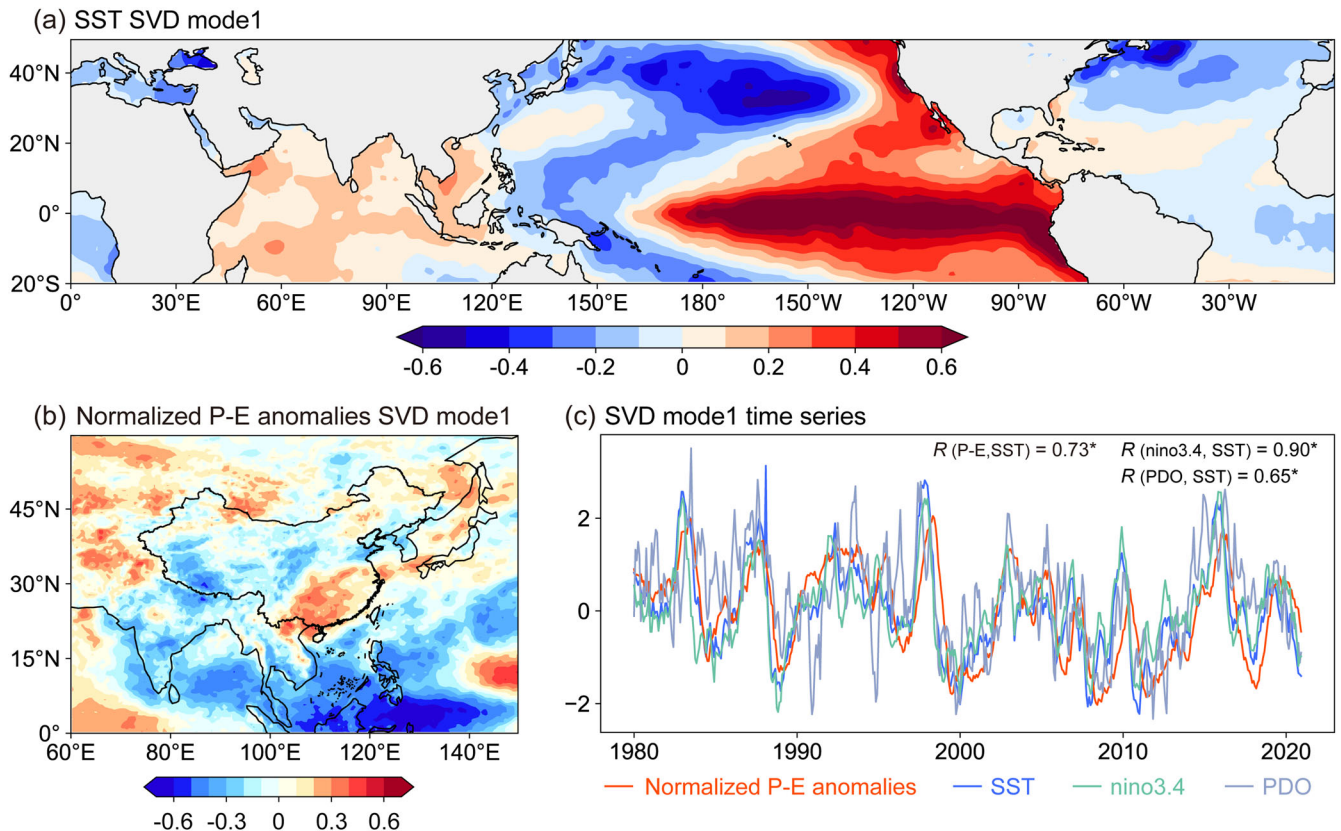


Fig. 3 Influences of SST on exogenous droughts in China. First Singular Value Decomposition (SVD) modes between the sea surface temperature (SST) and normalized PME anomalies during 1980–2020. **a**, **b** spatial pattern of SST and normalized PME anomalies; **c** normalized SVD time series of SST (blue lines), normalized PME anomalies (orange lines), PDO (grey lines) and Niño SST index 3.4 (green lines). Correlation coefficients (R) labelled with “*” are statistically significant at the 95% confidence level.

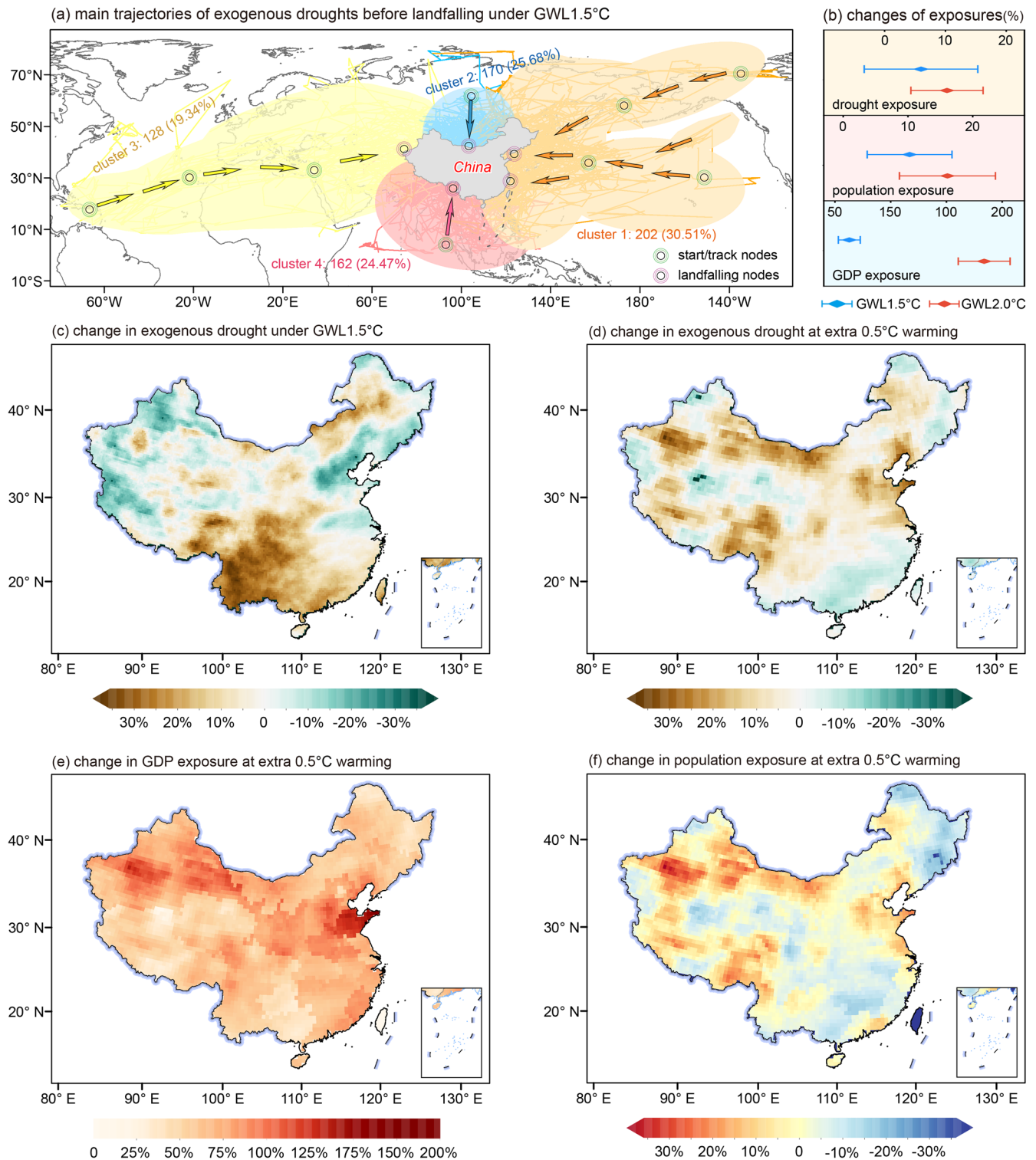


Fig. 4 Changes in exogenous drought and impacts at different GWLs under the SSP585 scenario. **a** Main routes of exogenous droughts at GWL 1.5°C. Colored lines show results of the k-means clustering while colored regions show the areas affected by exogenous drought transport. **b** Changes in exposure at different GWLs across China. Drought exposure is given as the average number of months per year that are exposed to drought. Population exposure is given as drought exposure times population. Similarly, GDP exposure is given as the product of drought exposure and regional contribution to GDP. Multi-model ensemble median changes (given in %) in exogenous drought exposure relative to the present-day level for GWL 1.5°C (**c**) and for the change between GWL 1.5°C and GWL 2°C (**d**). Difference between multi-model ensemble median population exposure (**e**) and GDP exposure (**f**) for GWL 1.5°C and GWL 2°C.

SSP245 and SSP485: -3 to +17%) (Fig. 4b, Supplementary Tables 1, 4). For GWL 2.0 °C, the expected increase is as high as 17 % (95% confidence interval: 9% to 34%). When comparing the projections of the two GWLs, we find substantial spatial variability in the drought exposure. While GWL 1.5 °C mainly results in increased exogenous drought exposure in the southern parts of eastern China, eastern QTP, and the eastern parts of northwestern China (Fig. 4c), GWL 2.0 °C exacerbates the exposure within the latitude band 30°N–40°N in all of China (Fig. 4d). In total, we estimate that GWL 2.0 °C would result in 12% to 21% more area to be exposed to exogenous droughts than with GWL 1.5 °C (Supplementary Table 4).

Given China's booming economy, we estimate that the GDP exposure would grow, on average, by around 55% (95% confidence interval: 39% to 69%) for GWL 1.5 °C (Supplementary Tables 3, 6) and by up to 185% (confidence interval: 88% to 204%) for GWL 2 °C. This means that additional warming from 1.5 °C to 2.0 °C would double the GDP exposure across China, with particularly prominent effects in the Shandong and Xinjiang provinces (Fig. 4e). Slightly less important numbers are found for the projected population exposure, which is nevertheless projected to increase, on average, by 7% (95% confidence interval: -3% to +15%) for GWL 1.5 °C and by 18% (7% to 21%) for GWL 2 °C (Supplementary Table 5). Also in this case, additional warming would result in additional exposure, with the exception of northeastern China and the provinces of Fujian, Jiangxi, and Hunan (Fig. 4f).

In summary, exogenous droughts would be amplifying across China (Supplementary Tables 1–6). An additional 1.5 °C or 2 °C warmer than pre-industrial levels (i.e., the average global air temperature during 1850–1900) increased socioeconomic exposure due to amplifying exogenous droughts. Comparatively, endogenous droughts would be alleviated over most regions of China. Limiting global warming to 1.5 °C rather than 2 °C would avoid 60% (53–66%) and 84% (50–137%) of exogenous drought exposure, 40.33% (38–72%) and 49.11% (34–113%) of population exposure, and 73% (45–72%) and 66.22% (65–71%) of economic exposure over China, under SSP245 and SSP585 scenarios, respectively.

DISCUSSION

Previous studies focusing on droughts often neglected external drivers such as the possible exogenous PME deficit^{6,40} or only focused on the oceanic vapor deficit¹⁵. Recent studies attempted to trace the evolution of droughts via moisture vapor transport^{15,16,41–44}, but doubts remain about the mechanistic linkages between drought occurrences and water vapor propagation, as well as about future tendencies. Our classification of droughts into exogenous and endogenous droughts allows for distinguishing four main propagation routes towards China, revealing that exogenous droughts accounted for 45% of all droughts that occurred in the coastal regions of China in the past (Fig. 1). This finding thus contributes to the understanding of regional droughts and might be leveraged for drought prediction.

Similarly, the earlier work suggests that the anomalous thermal forcing in the Southeast Asia and the Rossby wave train emerging over the North Atlantic are two prime drivers behind oceanic exogenous droughts⁴⁵. The latter mechanism is also linked to a positive potential height anomaly over Eurasia, aggravating the East Asian trough and the Siberian high^{45,46}, thus sustaining high pressure and resultant dry air subsidence. The anomalous thermal forcing, instead, is reflected anomalous convection induced by in SST oscillations. Such SST oscillations include the PDO and ENSO, and are believed to drive intense and widespread drying over China^{47–50}. The North Pacific SST mode with negative PDO phase has been proposed as the main driver behind exogenous droughts across China, and the PDO as the prime climate

modulator of precipitation in China^{47,50}. As PDO is a component of the Interdecadal Pacific Oscillation (IPO), the two oscillations follow similar variations⁵¹. Projected IPO trends⁵² indicate a shift towards less negative IPO phases during 2016–2051. Before the PDO shifts from predominantly negative to predominantly positive phases, however, increased SST variability in the equatorial eastern Pacific⁵³ may offset the effects of a lower IPO intensity. Based on our results, this could increase China's exposure to future exogenous droughts. It is a future work to further convince mechanisms of dry air mass transport process along with SST using GCM.

Current global average temperature is already 1.1 °C higher than pre-industrial levels, and the Paris Agreement's goal of limiting warming to 1.5 °C if possible, seems unrealistic at this stage⁵⁴. According to the SSP585 scenario we used, 1.5 °C and 2.0 °C of global warming will be reached in the 40-years periods centered around the years 2028 and 2042, respectively. These two periods coincide with negative phases of the PDO and occur just before a shift to a positive phase⁵². If it actually occurs, this PDO phase reversal after 2050 again weaken the impacts of exogenous droughts across China. Until then, however, the negative impacts of exogenous droughts would most effectively be alleviated by limiting global warming to 1.5 °C, rather than 2 °C.

With our work, we shed light in the mechanisms that lead to exogenous and endogenous droughts across China, especially along China's coastal regions (Fig. 1). We show that exogenous droughts accounted for almost half of the droughts that occurred along China's coastal regions in the recent past (Fig. 1b). Further, we backtrack the propagation trajectories of exogenous droughts towards China both during the period 1980–2020 and in future climate projections. We find that increasing exogenous drought exposure could increase drought risk, with consequences for both the local economy and population. For GWL 1.5 °C and across China, we estimate this increase to be in the order of 7% to 9% when compared to the historical period (Fig. 4b, Supplementary Tables 1, 4). Even higher exogenous drought exposure is found for GWL 2.0 °C (Fig. 4d). These findings call for reducing the level of additional warming as much as possible, and indicate the necessity for enhanced mitigation against future droughts.

METHODS

Observations and model simulations

The 0.25° × 0.25° gridded monthly precipitation and evapotranspiration data covering the period of 1979–2020 were sourced from the ERA5 reanalysis dataset⁵⁵, which is the latest release of the European Centre for Medium-Range Weather Forecasts' (ECMWF) fifth-generation Atmospheric reanalysis product.

The monthly SST dataset for the period 1980 to 2020 was acquired from the Hadley Centre⁵⁶, with a spatial resolution of 1.0° × 1.0°. We also obtained the time series of two climate indices from the Global Climate Observing System, i.e., the Pacific Decadal Oscillation (PDO) and the Nino3.4 SST index.

We used multi-model ensemble simulations from the Coupled Model Inter-comparison Project Phase 6 (CMIP6)^{57,58} to project the future changes of exogenous and endogenous droughts. The outputs of 12 global climate models (GCMs) from CMIP6 (ACCESS-CM2, ACCESS-ESM1-5, AWI-CM-1-1-MR, BCC-CSM2-MR, CAMS-CSM1-0, CMCC-CM2-SR5, CanESM5, FGOALS-g3, GFDL-ESM4, IPSL-CM6A-LR, MIROC6 and MRI-ESM2-0) provide precipitation and evapotranspiration time series (Supplementary Table 7). For future projections, CMIP6 combined Shared Socio-economic Paths (SSPs) and Representative Concentration Pathways (RCPs)⁵⁸. In this study, the historical simulations and two future scenarios (middle of the road SSP245 and fossil-fueled development SSP585) were examined. Given the coarse resolution of climate models and the variability in model simulations, we used (i) bilinear interpolation

for spatial disaggregation, and (ii) equidistant cumulative density function (ECDF) matching for bias correction. This allowed harmonizing the simulation model output to a resolution of 0.25° . This downscaling of the CMIP6 output resulted in an improved correlation with the reanalysis dataset ERA5 (Supplementary Figs. 20–22).

Gridded projections of GDP and population data

To investigate the exposure of both GDP and population to changes in exogenous and endogenous droughts, we used the gridded population and economic projection datasets of China³¹. These two datasets consider the newly-released two-child fertility policy as well as different SSPs. Both datasets come at a spatial resolution of $0.5^\circ \times 0.5^\circ$ and cover the period 2010–2100.

Identification and tracking of drought events

First, we calculated the precipitation minus evapotranspiration (PME) time series for each grid point and got the time series of monthly anomalies of PME over each grid cell by subtracting the respective calendar month mean (1980–2020 for ERA5, 1980–2014 for CMIP6) from each month's value. Then, we calculated moisture deficit based on 12-month cumulative anomalies of PME, and analyzed the impacts of PME on droughts. The contiguous areas defined by adjacent grid cells that show a 12-month cumulative anomalies of PME threshold below the 20% were defined as drought clusters if their area was in excess of $10,000 \text{ km}^2$. It is worth noting that we build empirical cumulative distributions using the time series of 12-month cumulative anomalies over each grid cell, and replace the value of each grid time series with the respective percentile. After defining such drought clusters, we characterized a single drought event as a 3-dimensional object with longitudinal and latitudinal extent, as well as time of occurrence. The 3-dimensional contiguous drought clusters with overlapping grid cells linked by the Lagrange tracking algorithm^{15,59} were defined as drought events. The drought clusters must last at least 3 months and we remove all clusters that last less than 3 months.

Droughts occurring in China were classified into exogenous and endogenous droughts (Supplementary Fig. 23). Exogenous drought includes terrestrial exogenous drought (exogenous drought transported overland) and oceanic exogenous drought (exogenous drought propagated from oceans). The aim was to dissect the droughts that occurred in China from an 'event-source' perspective. This allowed to (i) track the detected events along their trajectories, (ii) analyze the areas impacted by drought, and (iii) explore the spatial and temporal evolutions of their characteristics. This evolution was characterized based on the source location in the month prior to entry.

Since our study focuses on China, we define droughts as exogenous if the area affected by drought constitutes less than one third of the total drought area. Similarly, we define droughts as endogenous if more than two third of the drought area occur inside China. Drought events that do not satisfy any of the two conditions above are defined as "other" droughts. In addition, we define total droughts as the sum of exogenous droughts and endogenous droughts and others.

To quantify the similarity between different drought trajectories, we use the Hausdorff distance⁶⁰. All trajectories extracted from the models were clustered into four route categories using the k-means method. The clustering was also meant to increase the robustness of the analyses, as different models can provide different projections¹⁴. To characterize exogenous and endogenous droughts, we used drought frequency, drought exposure, and drought extent metrics as proposed by ref.¹⁵ (see Supplementary Table 8).

Geographic divisions and coastal regions in China

To discern between changes in drought characteristics within sub-regions, we considered three geographic divisions (Supplementary Fig. 24a) based on landform and climate regionalization: eastern China dominated by the Asian monsoon, northwestern China dominated by arid climate, and the Qinghai-Tibet Plateau (QTP). Eastern China was further divided into southern and northern parts along an imaginary line spanning from the Qinling Mountains to the Huaihe River basin. Coastal regions, finally, were defined as any Chinese provinces along shorelines (Supplementary Fig. 24b).

Definition of 1.5 °C and 2 °C global warming levels

We analyzed the changes and impacts of different global warming levels relative to the period 1975–2014 (present-day climatic conditions). The goal of the Paris Agreement is to limit global warming below 2°C , and if possibly below 1.5°C , compared to pre-industrial levels (period 1850–1900)⁶¹. Since the world will continue to warm in the coming decades, it is of significance to study the impacts, including the ones of exogenous droughts, under different GWLs. We analyze the two GWL 1.5 and 2.0°C , which we define as the first 40-year period for which a 40-year moving window of global temperature warming exceeded 1.5°C or 2.0°C relative to pre-industrial levels. We note that significant differences can occur in the timing of this period, depending on the considered climate model (Supplementary Table 9).

Definition of socio-economic exposure

The socio-economic exposure to a given hazard is not only affected by the change in hazard occurrence but also by the projected socio-economic changes⁶². To assess the extent to which socio-economics may be adversely affected by droughts, its exposure was quantified by multiplying the average number of months per year experiencing droughts (our drought-exposure metric) with the projected population or the projected GDP (two common socio-economic metrics). The unit of GDP exposure was thus "RMB*months/year", while the unit for population exposure is "inhabitants*months/year".

Definition of avoided impacts

We use the term "avoided impacts" to indicate the effects that can be avoided when achieving GWL 1.5°C instead of GWL 2.0°C ^{63,64}. Quantitatively, this effect is expressed as:

$$AI(\text{Avoided Impacts}) = \frac{C2.0 - C1.5}{C2.0} \times 100\% \quad (1)$$

wherein AI denotes the avoided impacts, and were C1.5 and C2.0 denote the change in a given metric (e.g., precipitation, GDP exposure, etc.) for GWL 1.5°C and GWL 2.0°C , respectively.

Singular value decomposition

Singular Value Decomposition (SVD), also known as Maximum Covariance Analysis (MCA), has been widely used in meteorology^{14,65} (SST anomalies and P-E anomalies in this study). In SVD, X and Y are the spatial matrices of SST and P-E anomalies with observation points m and q , respectively. The covariance matrix of two fields is S , and the number of time observations is N .

The spatial and temporal coefficients can be obtained as:

$$X = \begin{bmatrix} X_1(1) & \cdots & X_1(N) \\ \vdots & \ddots & \vdots \\ X_m(1) & \cdots & X_m(N) \end{bmatrix} \quad (2)$$

$$Y = \begin{bmatrix} Y_1(1) & \cdots & Y_1(N) \\ \vdots & \ddots & \vdots \\ Y_q(1) & \cdots & Y_q(N) \end{bmatrix} \quad (3)$$

$$S = \frac{1}{N}XY^T = UAV^T \quad (4)$$

$$PC_{x,m} = U_m^T X \quad (5)$$

$$PC_{y,m} = U_m^T Y \quad (6)$$

where A is the diagonal matrix of the singular value. From linear algebra, it is known that there exist unique U and V that maximize the covariance of the two fields. U and V are the spatial modes, respectively, for X and Y . $PC_{x,m}$ and $PC_{y,m}$ are the temporal coefficients for cells m in X and q in Y .

DATA AVAILABILITY

ERA5 data were obtained from <https://www.ecmwf.int/en/forecasts/datasets/reanalysis-datasets/era5>. The outputs of all GCMs used can be obtained from <https://esgf-node.llnl.gov/projects/cmip6>. HadISST data were obtained from <https://www.metoffice.gov.uk/hadobs/hadisst/data/download.html>. Time series of the Nino SST index 3.4 and PDO are available through https://psl.noaa.gov/gcos_wgsp/Timeseries/. Projected gridded GDP and population data can be obtained from Jiang's Group³².

CODE AVAILABILITY

The programming language Python was used to both analyze the data and creating the figures. All relevant codes are available from the corresponding author upon reasonable request.

Received: 2 August 2023; Accepted: 4 December 2023;

Published online: 21 December 2023

REFERENCES

- Jaeger, W. K. et al. Scope and limitations of drought management within complex human–natural systems. *Nat. Sustain.* **2**, 710–717 (2019).
- Overpeck, J. T. The challenge of hot drought. *Nature* **503**, 350–351 (2013).
- UNCCD Drought in numbers (UNCCD, 2016); <https://www.unccd.int/resources/publications/drought-numbers>.
- Dai, A. Increasing drought under global warming in observations and models. *Nat. Clim. Change* **3**, 52–58 (2013).
- Zhang, L. & Zhou, T. Drought over East Asia: A Review. *J. Clim.* **28**, 3375–3399 (2015).
- Yu, H. et al. Modified palmer drought severity index: model improvement and application. *Environ. Int.* **130**, 104951 (2019).
- Williams, A. P., Cook, B. I. & Smerdon, J. E. Rapid intensification of the emerging southwestern North American megadrought in 2020–2021. *Nat. Clim. Change* **12**, 232–234 (2022).
- Wise, E. K. Five centuries of U.S. West coast drought: occurrence, spatial distribution, and associated atmospheric circulation patterns. *Geophys. Res. Lett.* **43**, 4539–4546 (2016).
- Kingston, D. G., Stagge, J. H., Tallaksen, L. M. & Hannah, D. M. European-scale drought: understanding connections between atmospheric circulation and meteorological drought indices. *J. Clim.* **28**, 505–516 (2015).
- Pradhan, P., Costa, L., Rybski, D., Lucht, W. & Kropp, J. P. A systematic study of Sustainable Development Goal (SDG) Interactions. *Earth Future* **5**, 1169–1179 (2017).
- Lu, E., Luo, Y., Zhang, R., Wu, Q. & Liu, L. Regional atmospheric anomalies responsible for the 2009–2010 severe drought in China. *J. Geophys. Res. Atmos.* **116** (2011).
- Cai, W., Cowan, T., Briggs, P. & Raupach, M. Rising temperature depletes soil moisture and exacerbates severe drought conditions across southeast Australia. *Geophys. Res. Lett.* **36**, L21709 (2009).
- Zhang, Q. et al. Nonparametric integrated agrometeorological drought monitoring: model development and application. *J. Geophys. Res. Atmos.* **123**, 73–88 (2018).
- Shen, Z. et al. Drying in the low-latitude Atlantic Ocean contributed to terrestrial water storage depletion across Eurasia. *Nat. Commun.* **13**, 1849 (2022).
- Herrera-Estrada, J. E. & Diffenbaugh, N. S. Landfalling droughts: global tracking of moisture deficits from the oceans onto land. *Water Resour. Res.* **56**, e2019WR026877 (2020).
- Herrera-Estrada, J. E. et al. Reduced moisture transport linked to drought propagation across North America. *Geophys. Res. Lett.* **46**, 5243–5253 (2019).
- Schubert, S. D. et al. Global meteorological drought: a synthesis of current understanding with a focus on SST drivers of precipitation deficits. *J. Clim.* **29**, 3989–4019 (2016).
- Schumacher, D. L., Keune, J., Dirmeyer, P. & Miralles, D. G. Drought self-propagation in drylands due to land–atmosphere feedbacks. *Nat. Geosci.* **15**, 262–268 (2022).
- Ault, T. R. On the essentials of drought in a changing climate. *Science* **368**, 256–260 (2020).
- Zhou, S. et al. Land-atmosphere feedbacks exacerbate concurrent soil drought and atmospheric aridity. *Proc. Natl Acad. Sci. USA* **116**, 18848–18853 (2019).
- Berg, A. et al. Land–atmosphere feedbacks amplify aridity increase over land under global warming. *Nat. Clim. Change* **6**, 869–874 (2016).
- Sherwood, S. & Fu, Q. A drier future? *Science* **343**, 737–739 (2014).
- Hassan, W. U. & Nayak, M. A. Global teleconnections in droughts caused by oceanic and atmospheric circulation patterns. *Environ. Res. Lett.* **16**, 014007 (2020).
- King, A. D., Pitman, A. J., Henley, B. J., Ukkola, A. M. & Brown, J. R. The role of climate variability in Australian drought. *Nat. Clim. Change* **10**, 177–179 (2020).
- Nangombe, S. et al. Record-breaking climate extremes in Africa under stabilized 1.5°C and 2°C global warming scenarios. *Nat. Clim. Change* **8**, 375–380 (2018).
- Qiu, J. China drought highlights future climate threats. *Nature* **465**, 142–143 (2010).
- Li, C. et al. Drivers and impacts of changes in China's drylands. *Nat. Rev. Earth Environ.* **2**, 858–873 (2021).
- Lü, J., Ju, J., Ren, J. & Gan, W. The influence of the Madden-Julian Oscillation activity anomalies on Yunnan's extreme drought of 2009–2010. *Sci. China Earth Sci.* **55**, 98–112 (2012).
- Wang, S., Yuan, X. & Li, Y. Does a strong El Niño imply a higher predictability of extreme drought? *Sci. Rep.* **7**, 40741 (2017).
- Ren, Q. et al. Impacts of urban expansion on natural habitats in global drylands. *Nat. Sustain.* **5**, 869–878 (2022).
- Huang, J. et al. Effect of fertility policy changes on the population structure and economy of China: from the perspective of the shared socioeconomic pathways. *Earth Future* **7**, 250–265 (2019).
- National Bureau of Statistics of China, *China statistical yearbook* 2018. (China Statistics Press).
- Zhang, C. Moisture sources for precipitation in Southwest China in summer and the changes during the extreme droughts of 2006 and 2011. *J. Hydrol.* **591**, 125333 (2020).
- Basconcello, J. & Moon, I.-J. Increasing activity of tropical cyclones in East Asia during the mature boreal autumn linked to long-term climate variability. *npj Clim. Atmos. Sci.* **5**, 4 (2022).
- Huang, J., Yu, H., Guan, X., Wang, G. & Guo, R. Accelerated dryland expansion under climate change. *Nat. Clim. Change* **6**, 166–171 (2016).
- Huang, J. et al. Dryland climate change: recent progress and challenges. *Rev. Geophys.* **55**, 719–778 (2017).
- Gu, X. et al. Intensification and expansion of soil moisture drying in warm season over Eurasia under global warming. *J. Geophys. Res. Atmos.* **124**, 3765–3782 (2019).
- Pokhrel, Y. et al. Global terrestrial water storage and drought severity under climate change. *Nat. Clim. Change* **11**, 226–233 (2021).
- Yang, W. et al. Human intervention will stabilize groundwater storage across the north China plain. *Water Resour. Res.* **58**, e2021WR030884 (2022).
- Hao, Z., Singh, V. P. & Xia, Y. Seasonal drought prediction: advances, challenges, and future prospects. *Rev. Geophys.* **56**, 108–141 (2018).
- Sun, C. & Yang, S. Persistent severe drought in southern China during winter-spring 2011: Large-scale circulation patterns and possible impacting factors. *J. Geophys. Res. Atmos.* **117**, D10112 (2012).
- Singh, J. et al. Enhanced risk of concurrent regional droughts with increased ENSO variability and warming. *Nat. Clim. Change* **12**, 163–170 (2022).
- Satoh, Y. et al. The timing of unprecedented hydrological drought under climate change. *Nat. Commun.* **13**, 3287 (2022).

44. Hoerling, M. et al. Causes and predictability of the 2012 great plains drought. *Bull. Am. Meteorol. Soc.* **95**, 269–282 (2014).
45. Jin, D., Guan, Z. & Tang, W. The extreme drought event during winter–spring of 2011 in East China: combined influences of teleconnection in mid-high latitudes and thermal forcing in maritime continent region. *J. Clim.* **26**, 8210–8222 (2013).
46. Li, H., He, S., Gao, Y., Chen, H. & Wang, H. North Atlantic modulation of inter-decadal variations in hot drought events over northeastern China. *J. Clim.* **33**, 4315–4332 (2020).
47. Apurv, T., Xu, Y.-P., Wang, Z. & Cai, X. Multidecadal changes in meteorological drought severity and their drivers in mainland China. *J. Geophys. Res. Atmos.* **124**, 12937–12952 (2019).
48. Ma, F., Yuan, X. & Ye, A. Seasonal drought predictability and forecast skill over China. *J. Geophys. Res. Atmos.* **120**, 8264–8275 (2015).
49. Qian, C., Yu, J.-Y. & Chen, G. Decadal summer drought frequency in China: the increasing influence of the Atlantic Multi-decadal Oscillation. *Environ. Res. Lett.* **9**, 124004 (2014).
50. Yu, E., King, M. P., Sobolowski, S., Otterå, O. H. & Gao, Y. Asian droughts in the last millennium: a search for robust impacts of the Pacific Ocean surface temperature variabilities. *Clim. Dyn.* **50**, 4671–4689 (2018).
51. Qin, M., Li, D., Dai, A., Hua, W. & Ma, H. The influence of the Pacific Decadal Oscillation on North Central China precipitation during boreal autumn. *Int. J. Climatol.* **38**, e821–e831 (2018).
52. Wu, M. et al. A very likely weakening of Pacific Walker Circulation in constrained near-future projections. *Nat. Commun.* **12**, 6502 (2021).
53. Cai, W. et al. Increased ENSO sea surface temperature variability under four IPCC emission scenarios. *Nat. Clim. Change* **12**, 228–231 (2022).
54. Armstrong McKay, D. I. et al. Exceeding 1.5°C global warming could trigger multiple climate tipping points. *Science* **377**, eabn7950 (2022).
55. Hersbach, H. et al. The ERA5 global reanalysis. *Q. J. Roy. Meteor. Soc.* **146**, 1999–2049 (2020).
56. Rayner, N. A. et al. Global analyses of sea surface temperature, sea ice, and night marine air temperature since the late nineteenth century. *J. Geophys. Res. Atmos.* **108**, 4407 (2003).
57. Eyring, V. et al. Overview of the Coupled Model Intercomparison Project Phase 6 (CMIP6) experimental design and organization. *Geosci. Model Dev.* **9**, 1937–1958 (2016).
58. O'Neill, B. C. et al. The Scenario Model Intercomparison Project (ScenarioMIP) for CMIP6. *Geosci. Model Dev.* **9**, 3461–3482 (2016).
59. Herrera-Estrada, J. E., Satoh, Y. & Sheffield, J. Spatiotemporal dynamics of global drought. *Geophys. Res. Lett.* **44**, 2254–2263 (2017).
60. Taha, A. A. & Hanbury, A. An efficient algorithm for calculating the exact Harsdorf distance. *IEEE Trans. Pattern Anal. Mach. Intell.* **37**, 2153–2163 (2015).
61. Gillett, N. P. et al. Constraining human contributions to observed warming since the pre-industrial period. *Nat. Clim. Change* **11**, 207–212 (2021).
62. Russo, S. et al. Half a degree and rapid socioeconomic development matter for heatwave risk. *Nat. Commun.* **10**, 136 (2019).
63. Wang, G., Zhang, Q., Yu, H., Shen, Z. & Sun, P. Double increase in precipitation extremes across China in a 1.5 °C/2.0 °C warmer climate. *Sci. Total Environ.* **746**, 140807 (2020).
64. Rodrigues, R. R., Taschetto, A. S., Sen Gupta, A. & Foltz, G. R. Common cause for severe droughts in South America and marine heatwaves in the South Atlantic. *Nat. Geosci.* **12**, 620–626 (2019).
65. Takaya, K. & Nakamura, H. A formulation of a phase-independent wave-activity flux for stationary and migratory quasigeostrophic eddies on a zonally varying basic flow. *J. Atmos. Sci.* **58**, 608–627 (2001).

ACKNOWLEDGEMENTS

G.W. and Q.Z. acknowledge the support from the China National Key R&D Program (Grant No. 2019YFA0606900). We would like to thank the high-performance computing support from the Center for Geodata and Analysis, Faculty of Geographical Science, Beijing Normal University [<https://gda.bnu.edu.cn/>]. Here we would like to thank the Editor in Chief, Prof. Roy Harrison, and anonymous reviewers for their professional and pertinent comments and suggestions which are greatly helpful for further quality improvement of this manuscript.

AUTHOR CONTRIBUTIONS

G.W. and Q.Z. designed the study and wrote the manuscript, with contributions from D.F., and G.W. performed the analysis. G.W., Q.Z., Y.P., D.F., J.W., V.S. and C.X. discussed and modified the manuscript. All authors contributed to the interpretation of the results.

COMPETING INTERESTS

The authors declare no competing interests.

ADDITIONAL INFORMATION

Supplementary information The online version contains supplementary material available at <https://doi.org/10.1038/s41612-023-00543-8>.

Correspondence and requests for materials should be addressed to Qiang Zhang.

Reprints and permission information is available at <http://www.nature.com/reprints>

Publisher's note Springer Nature remains neutral with regard to jurisdictional claims in published maps and institutional affiliations.



Open Access This article is licensed under a Creative Commons Attribution 4.0 International License, which permits use, sharing, adaptation, distribution and reproduction in any medium or format, as long as you give appropriate credit to the original author(s) and the source, provide a link to the Creative Commons license, and indicate if changes were made. The images or other third party material in this article are included in the article's Creative Commons license, unless indicated otherwise in a credit line to the material. If material is not included in the article's Creative Commons license and your intended use is not permitted by statutory regulation or exceeds the permitted use, you will need to obtain permission directly from the copyright holder. To view a copy of this license, visit <http://creativecommons.org/licenses/by/4.0/>.

© The Author(s) 2023